buildings

MDPI

Article

Synergistic Effects of Carbonated and Hydrophobically Modified Municipal Solid Waste Incineration Fly Ash on Mortar Performance and Heavy-Metal Immobilisation

Jingwei Zhang [1], Yi Zheng [1], Kangjie Zhang [2,*] and Jia Li [2]

[1] School of Civil Engineering, Zhengzhou University, Zhengzhou 450001, China; zhangjingwei@zzu.edu.cn (J.Z.); zhengyi2021@gs.zzu.edu.cn (Y.Z.)
[2] School of Water Conservancy and Transportation, Zhengzhou University, Zhengzhou 450001, China; lijia@zzu.edu.cn
* Correspondence: kangjiezhang@gs.zzu.edu.cn

Abstract

Municipal solid waste incineration (MSWI) fly ash contains soluble salts and heavy metals, which may cause leaching risks and durability deterioration when directly used in cement-based materials. This study aimed to investigate the synergistic effects of carbonated and hydrophobically modified municipal solid waste incineration fly ashes on the engineering performance and heavy-metal immobilisation of mortar. Mortars containing modified fly ashes were evaluated in terms of hydration behavior, compressive strength, water absorption, electrically accelerated corrosion resistance, heavy metal leaching, and microstructure. Carbonated fly ash promoted hydration through the nucleation and filling effects of $CaCO_3$, shortened setting time, increased cumulative hydration heat, and improved compressive strength by up to 4.5 MPa. Hydrophobic fly ash reduced particle wettability and capillary water transport, thereby reducing water uptake and mitigating visible corrosion-induced deterioration under accelerated conditions, although excessive dosage delayed hydration and reduced strength. The combined modification showed a clear synergistic effect, reducing water absorption by up to 39.9%. In particular, the C3H3 specimen, containing 75 kg·m^{-3} carbonated MSWI fly ash and 75 kg·m^{-3} hydrophobically modified MSWI fly ash, exhibited the lowest water absorption of 3.92% and effectively suppressed crack propagation and corrosion-product migration. The leaching concentrations of Cr, Cu, Zn, As, Cd, and Pb were below the GB 18598—2019 limits. X-ray diffraction (XRD), Fourier-transform infrared spectroscopy (FTIR), thermogravimetric analysis (TG), and low-field nuclear magnetic resonance (NMR) results indicated that the improved performance originated from a composite barrier involving carbonate filling, hydrophobic interfacial blocking, and heavy metal solidification/stabilization.

Keywords: municipal solid waste incineration fly ash; carbonation modification; hydrophobic modification; synergistic effect; heavy metal leaching

Academic Editor: Salvatore Verre

Received: 31 May 2026
Revised: 21 June 2026
Accepted: 25 June 2026
Published: 29 June 2026

1. Introduction

With economic development, population agglomeration, and changes in urban lifestyles, the generation of municipal solid waste (MSW) has continued to increase, and its safe and efficient disposal has become a major issue in urban environmental governance [1,2]. Incineration, as a mainstream approach for municipal solid waste treatment, can reduce waste volume by approximately 90% and mass by 75–80%, while enabling heat

and power generation through waste heat recovery [3]. However, this process inevitably generates municipal solid waste incineration fly ash (MSWI FA) [4]. MSWI fly ash is the fine residue captured by air-pollution-control systems during municipal solid waste incineration [5]. Unlike conventional coal fly ash, it is more heterogeneous and generally poses greater environmental risks, necessitating appropriate pretreatment before its utilisation in cement-based materials. In recent years, the total amount of solid waste generated in China has approached 10 billion tonnes, of which combustion-derived wastes account for approximately 350 million tonnes [6,7]. The annual global generation of MSWI fly ash has exceeded 10 million tonnes [8,9]. MSWI fly ash is rich in potentially cementitious components, such as Ca, Si, Al, and Fe; however, it also contains hazardous substances, including heavy metals such as Pb, Cd, Cr, and Cu, high levels of soluble chloride salts, and dioxins. In particular, the chloride content introduced by kitchen waste can reach 15–20%, which may give rise to a series of environmental and durability-related problems [10,11]. Therefore, in the context of zero-waste cities and green, low-carbon circular development, there is an urgent need to explore pathways for the safe stabilisation and resource utilisation of MSWI fly ash [12].

Existing MSWI fly ash treatments can be broadly classified into desalination, activation, and densification. Desalination mainly includes water washing, electrodialysis, and acid washing. Under a liquid-to-solid ratio of 8:1, a washing time of 5 min, and 70 °C, chloride removal can reach 88.72% [13,14]. Water washing promotes the dissolution of soluble salts [15], while electrodialysis further removes mobile salts and some metals [16]. However, washing may generate saline wastewater, alter fly ash chemistry and surface structure, and remains less effective for poorly soluble chlorides and heavy metals [17,18]. Activation improves the reactivity of MSWI fly ash through mechanical grinding and chemical treatment [19]. Mechanochemical pretreatment refines particles, creates structural defects, and promotes the release of reactive components [20]. When combined with CO_2 mineralisation, it increases the 28 d compressive strength of mortar by 43.6% and reduces the leaching of As, Ba, Ni, Pb, Se, and Zn by 17.9–77.8% [21].

Densification includes cement-based solidification, geopolymerisation, carbonation, and high-temperature sintering. Pressure-assisted sintering promotes chloride migration and mineral reconstruction [22], while high-temperature treatment reduces fly ash toxicity and improves its suitability as a cementitious material [23]. Sintering at 1150 °C reduces heavy-metal leaching by 62.50%, but requires substantial energy and may cause metal volatilisation [24]. By contrast, carbonation fixes CO_2 through reactions with CaO and $Ca(OH)_2$, while carbonate precipitation reduces free alkalis, fills pores, and stabilises heavy metals [25,26]. After 6 h of accelerated carbonation, the calcite content increases by 67%, and Cu and Pb leaching decreases by 53.1% and 73.5%, respectively [27]. Because no single method can simultaneously achieve low cost, low energy demand, performance improvement, and long-term environmental safety, combined treatment has become an important direction for MSWI fly ash utilisation.

In addition to chemical stabilisation and pore densification, moisture transport is another key factor affecting the long-term environmental safety of MSWI fly ash. MSWI fly ash usually contains high levels of chlorides. With the increasing frequency of extreme rainfall events, the service performance of fly ash-based cementitious materials is highly susceptible to water transport and the migration of aggressive media [28,29]. Once water penetrates into the pores of mortar, it can not only promote the migration of corrosive ions and induce the leaching of heavy metals, but also aggravate pore structure deterioration, matrix cracking, and reinforcement corrosion [30–32]. In particular, MSWI fly ash particles are generally characterised by rough, porous, and highly water-absorptive features; therefore, their direct incorporation into mortar may increase the water absorption

capacity of the system and weaken the impermeability and durability of the material [33]. Hydrophobic modification can reduce the hydrophilicity of fly ash particles by introducing low-surface-energy groups or forming hydrophobic films on their surfaces, thereby inhibiting water uptake and the transport of aggressive ions, and mitigating pollutant migration in water and material deterioration at the source [34–36].

A single treatment method is difficult to satisfy the requirements of fly ash-based mortar in terms of mechanical performance, resistance to water-induced deterioration, and environmental safety. Carbonation-modified fly ash can improve the stability of fly ash through mineral phase transformation and carbonate precipitation, whereas hydrophobically modified fly ash can enhance the durability of mortar by inhibiting the migration of water and aggressive ions. The synergistic effect of these two modification strategies in cementitious systems may provide a new pathway for the high-volume, safe, and functional utilisation of MSWI fly ash. However, studies on the effects of the combined incorporation of carbonation-modified and hydrophobically modified fly ash into mortar on the hydration process, pore structure, water absorption behaviour, mechanical properties, corrosion resistance, and heavy metal immobilisation remain limited. Therefore, in this study, mortars incorporating both hydrophobically modified and carbonated MSWI fly ash were prepared, and their mechanical properties, hydration heat, water absorption, corrosion resistance, heavy metal leaching, hydration products, and pore structure were systematically evaluated. The mechanisms by which carbonation stabilisation and hydrophobic blocking improve mortar performance were further elucidated, which is of great significance for enhancing the long-term service performance of mortars prepared with municipal solid waste incineration fly ash.

2. Materials and Methods

2.1. Materials

R·SAC 42.5 sulphoaluminate cement (SAC), P.O 42.5 ordinary Portland cement (OPC), silica fume (SF), unmodified MSWI fly ash (WF), hydrophobically modified MSWI fly ash (HWF), and carbonated MSWI fly ash (CWF) were used as raw materials, while quartz sand was used as the aggregate. R·SAC 42.5, P.O 42.5 and quartz sand were supplied by Zhengzhou Jingwei Building Materials Co., Ltd., Longwowa Village, Jiayu Town, Xingyang City, Henan Province, China. Silica fume was supplied by Luoyang Yumin Microsilica Powder Co., Ltd., China, while the MSWI fly ash was collected from the Xingjin Waste Incineration Plant in Zhengzhou, China. The main components of SAC were anhydrous calcium sulphoaluminate (C_4A_3S, 56.2%) and dicalcium silicate (C_2S, 26.2%). The ordinary Portland cement was mainly composed of tricalcium silicate (C_3S, 57.3%), dicalcium silicate (C_2S, 23.5%), tricalcium aluminate (C_3A, 6.5%), and tetracalcium aluminoferrite (C_4AF, 10.5%).

The preparation procedure for carbonated MSWI fly ash was as follows. First, MSWI fly ash was mixed with water at a mass ratio of 1:5 for washing. Water washing can remove soluble salts and reduce the chloride content in fly ash [37]. A lower chloride content is beneficial for improving the thermal stability of the material [38]. The washed fly ash was dried in an oven at 60 °C, after which the dried material was placed in a carbonation chamber. The carbonation conditions were set as follows: temperature of 25 °C, CO_2 concentration of 5%, pressure of 0.1 MPa, and carbonation duration of 1 day. The preparation procedure for hydrophobically modified MSWI fly ash was as follows. Acetic acid was added dropwise into an ethanol solution to adjust the pH to 4–5. Deionised water and methyltrimethoxysilane (MTMS, Shanghai Yien Chemical Technology Co., Ltd., China) were then added and mixed thoroughly, followed by sufficient stirring to promote silane hydrolysis. Subsequently, MSWI fly ash, deionised water, and surfactant were added

to the mixture at a ratio of 10:20:1, and the suspension was continuously stirred on a magnetic stirrer at 90 °C for 4 h, allowing the hydrolysis products of silane to bond with the MSWI fly ash. The hydrophobically modified MSWI fly ash was subsequently oven-dried at 105 °C for 12 h to obtain the final product.

The morphologies of the raw materials are shown in Figure 1, and the XRF results of the three types of MSWI fly ash are presented in Table 1. The main mineral phases in the original MSWI fly ash included SiO_2, $CaCO_3$, $CaSO_4$, $Ca(OH)_2$, CaClOH, NaCl, and KCl, with Ca, Si, O, and Cl being the dominant elements. After carbonation, the chloride content of the CWF decreased, which was attributed to the removal of soluble salts during the washing process. The increased SiO_2 content of HWF was attributed to the introduction of Si-containing siloxane species derived from methyltrimethoxysilane.

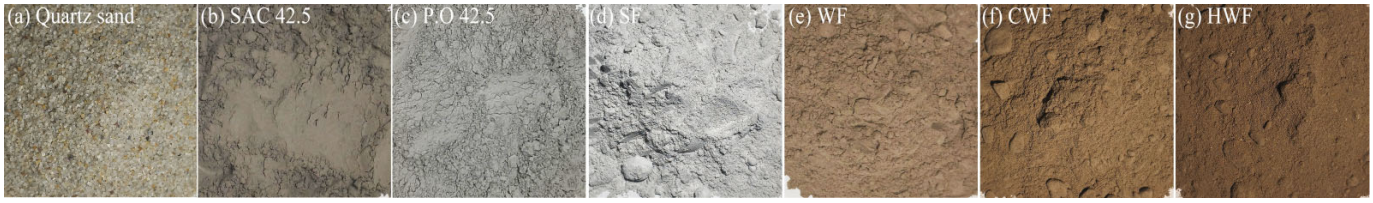

Figure 1. Morphologies of the raw materials.

Table 1. XRF of Three Types of Waste Fly Ash.

Chemical Composition	CaO	SiO_2	Cl	Na_2O	Al_2O_3	SO_3	P_2O_5	Fe_2O_3	MgO	K_2O	TiO_2	ZnO	CuO	Cr_2O_3	Others
WF	33.9	16.7	9.7	8.9	8.2	4.4	4.3	4.1	3.8	2.9	1.4	0.5	0.2	0.1	0.3
CWF	34.9	17.0	7.9	6.6	9.2	4.9	4.1	4.6	3.3	3.4	1.2	0.7	0.2	0.1	1.1
HWF	34.3	28.5	4.1	3.1	8.2	4.3	3.6	4.8	3.1	2.4	1.4	0.8	0.2	0.1	0.6

The particle size distributions of the raw materials are shown in Figure 2a. The mean particle sizes of sulphoaluminate cement, ordinary Portland cement, silica fume, MSWI fly ash, hydrophobically modified MSWI fly ash, carbonated MSWI fly ash, and quartz sand were 4.38 μm, 13.58 μm, 6.08 μm, 11.72 μm, 36.69 μm, 43.67 μm, and 474.69 μm, respectively. After hydrophobic and carbonation modification, the particle size of MSWI fly ash increased markedly compared with that of the original material, indicating that both grafted functional groups and carbonation treatment contributed to the enlargement of fine particles.

The XRD patterns and static water contact angles of the three MSWI fly ashes are shown in Figure 2b, and their FTIR spectra are presented in Figure 2c. WF mainly contained SiO_2, $CaCO_3$, $CaSO_4$, $Ca(OH)_2$, CaClOH, NaCl, and KCl. Compared with WF, CWF exhibited stronger $CaCO_3$ diffraction peaks and CO_3^{2-} absorption bands at approximately 1420 and 870 cm^{-1}, confirming the formation of additional carbonate products during carbonation. The water contact angle increased from 26.8° for WF to 147.2° for HWF, indicating substantially reduced surface wettability. Moreover, the C–H bands at 2918 and 2850 cm^{-1} and the Si–CH_3 band near 1260 cm^{-1} indicated the introduction of methylsiloxane groups onto the HWF surface. These results verify the effectiveness of both carbonation and hydrophobic modification.

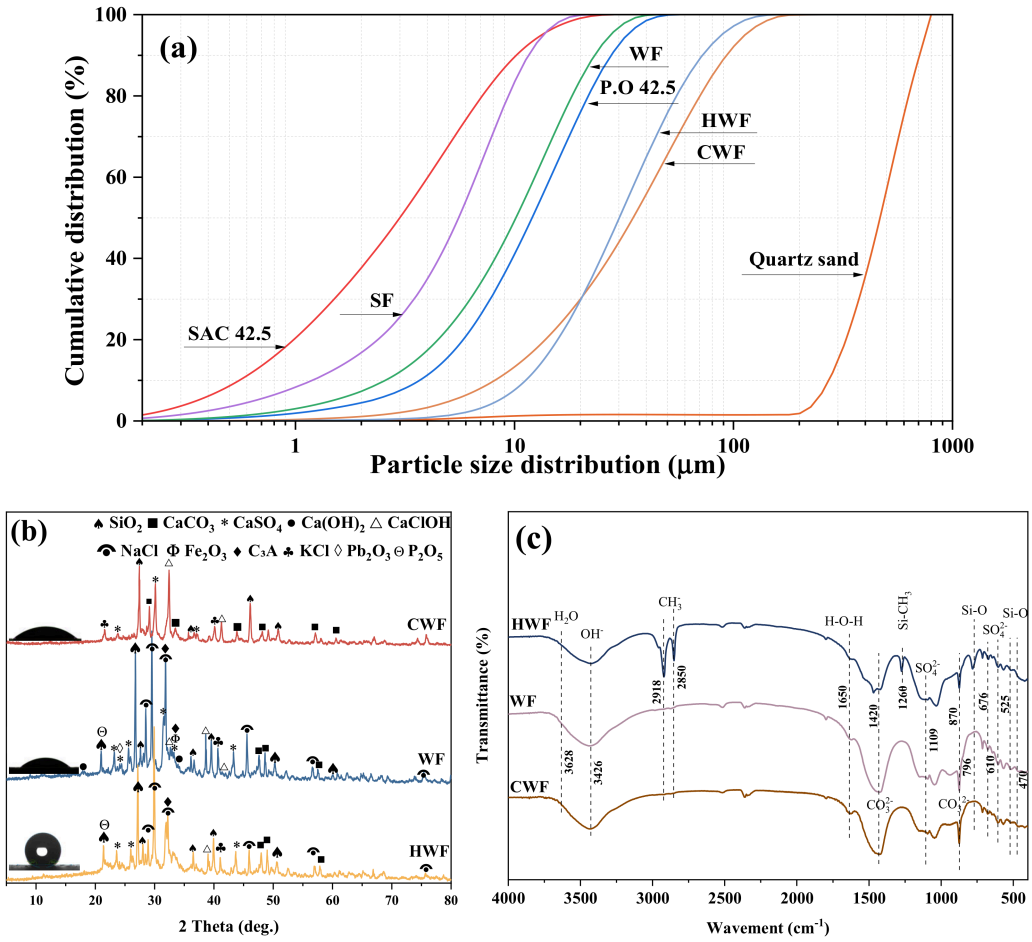

Figure 2. (**a**) Particle size of raw materials; (**b**) XRD results and static water contact angles of the three types of waste fly ash; (**c**) FTIR spectra of the three types of waste fly ash.

2.2. Mix Proportion Design and Specimen Preparation

The mix proportions of mortars prepared with MSWI fly ash are presented in Table 2. The mixture proportions were determined based on preliminary tests and previous studies on MSWI fly ash mortars [39]. Earlier studies employed MSWI fly ash dosages of up to 140 kg·m^{-3} [40] and adopted blended calcium sulphoaluminate cement–ordinary Portland cement systems [41]. The mass ratio of cementitious materials to fine aggregate was 1:1, and the water-to-binder ratio was 0.30. The dosage of MSWI fly ash accounted for approximately 15% of the total mass of cementitious materials. CW0 was the reference mixture containing unmodified MSWI fly ash, whereas CW6 and HW6 contained only carbonated and hydrophobically modified MSWI fly ash, respectively. The CWF-to-HWF mass ratios in C4H2, C3H3, and C2H4 were 2:1, 1:1, and 1:2, representing CWF-dominated, equal-proportion, and HWF-dominated systems, respectively. This design enabled the individual and synergistic effects of the two modifications to be compared at a constant total MSWI fly ash content. Hydrophobic-modified MSWI fly ash and carbonated MSWI fly ash were used either in combination or individually to replace unmodified MSWI fly ash. The superplasticizer (Jiangsu Subote New Materials Co., Ltd.,China) dosage was 0.3% by mass of the cementitious materials.

Mortar preparation, casting, and curing were conducted in accordance with GB/T 17671-2021 [42]. Prismatic specimens measuring 40 × 40 × 160 mm were used for the compressive-strength test, while cubic specimens measuring 40 × 40 × 40 mm were used for the water-absorption test. The cementitious materials were dry-mixed for 2 min, after which premixed water and superplasticiser were added and mixed at low speed for

2 min. Quartz sand was then introduced, followed by high-speed mixing for 2 min, a 60 s pause for scraping, and a further 1 min of mixing. The fresh mortar was cast and vibrated, demoulded after 24 h, and cured at 20 ± 2 °C and a relative humidity of at least 95% until testing.

Table 2. Mix ratios of mortar with different waste fly ash (kg/m^3).

Samples	SAC 42.5	P.O 42.5	SF	WF	CWF	HWF	Quartz Sand	Water	SP
CW0	526	222	82	150	0	0	980	294	3
CW6	526	222	82	0	150	0	980	294	3
HW6	526	222	82	0	0	150	980	294	3
C4H2	526	222	82	0	100	50	980	294	3
C3H3	526	222	82	0	75	75	980	294	3
C2H4	526	222	82	0	50	100	980	294	3

Note: CW0 denotes the reference group. CW and C denote samples containing carbonated MSWI fly ash, while HW and H denote samples containing hydrophobic-modified MSWI fly ash. CW6 indicates the incorporation of carbonated MSWI fly ash at 150 kg/m^3. C4H2 indicates that the dosages of carbonated MSWI fly ash and hydrophobic-modified MSWI fly ash were 100 kg/m^3 and 50 kg/m^3, respectively. C3H3 indicates that both carbonated MSWI fly ash and hydrophobic-modified MSWI fly ash were incorporated at 75 kg/m^3.

2.3. Macroscopic and Microscopic Characterisation

The setting time of the mortar was determined using a Vicat apparatus in accordance with the Chinese standard GB/T 1346-2011 [43]. The compressive strength of the mortar was tested according to the Chinese standard GB/T 17671-2021 [42]. For each mixture and curing age, compressive strength is reported as the mean ± standard deviation of (n) replicate measurements. The heat of hydration was measured in accordance with ASTM C1679 [44]. Cement pastes with the mix proportions listed in Table 2 were prepared, and their heat flow and cumulative heat release were measured using a conduction isothermal calorimeter (TAM Air, TA Instruments, USA). The test temperature was maintained at 20 °C, and data were recorded continuously for 72 h. The water absorption of the mortar was measured in accordance with the Chinese standard GB/T 50081-2019 [45]. For the water absorption test, the mortar specimens cured for 28 d were first dried to constant mass. The specimens were then completely immersed in water, with the water level maintained 25 mm above the top surface of the specimens. The mass of the specimens was continuously measured at different immersion times within 5 d. The electrically accelerated corrosion test was conducted using a 220 V direct-current regulated power supply (MT-152D, Maisheng, China) [46]. The steel bar embedded in the mortar was used as the anode and connected to the positive terminal of the power supply, while a copper sheet immersed in the external solution was used as the auxiliary electrode and connected to the negative terminal. Each specimen was connected to an independent power supply. Before electrification, the mortar specimens were immersed in a 5% NaCl solution for 24 h to ensure complete wetting [47]. Subsequently, the immersed specimens were placed in a 5% NaCl solution, and the liquid level was adjusted to slightly below the upper surface of the specimens. The applied voltage was controlled at 8 V for 8 d, with electrification conducted for 12 h per day. A freshly prepared NaCl solution was used before electrification each day. The corrosion resistance of the mortar was characterised by observing the morphology of the embedded steel bars. The externally applied potential accelerates electrochemical reactions and may alter current distribution, chloride transport, oxygen availability, and the development of corrosion products compared with natural chloride exposure. Therefore, the electrically accelerated corrosion test was used as a comparative screening method to evaluate the corrosion-related behaviour of different mortar mixtures under identical test conditions.

The heavy metal contents in the mortars were determined by ICP-MS. After standard curing for 28 d, the specimens were crushed, and powder samples with particle sizes smaller than 1 mm were sieved for analysis. After weighing, the samples were subjected to microwave digestion using aqua regia (HCl:HNO_3 = 3:1) at 180 °C to ensure sufficient release of metal elements from the specimens [48]. The digested solutions were filtered through a 0.22 μm PTFE membrane, diluted to a fixed volume, and then analyzed using an inductively coupled plasma mass spectrometer (Agilent 7900, Agilent Technologies, USA) to determine the contents of Pb, Cr, As, Cd, Zn, Cu, and other elements. During the analysis, Rh, In, and Ge were used as internal standard elements to correct for matrix effects and instrumental signal drift.

After curing for 28 d, representative fragments were collected from different locations of the mortar specimens in each group, then crushed, dried, ground, and thoroughly homogenised to prepare powder samples for XRD, FTIR, and TG analyses. Powder samples with particle sizes below 75 μm were used for both XRD (D8 Advance, Bruker, Germany) and FTIR (Nicolet iS50, Thermo Scientific, USA) analyses. For XRD analysis, the 2θ range and scanning rate were 10–80° and 0.5°/min, respectively. For FTIR analysis, the wavenumber range was 400–4000 cm^{-1}. Thermogravimetric analysis was conducted using a thermal analyser (STA 8000, PerkinElmer, USA). Powder samples below 45 μm were used for TG analysis, with a temperature range of 25–800 °C and a heating rate of 10 °C/min. The pore structure of the mortar was characterised using a low-field nuclear magnetic resonance analyser (MesoMR12-060, NIUMAG). The intensity of the NMR signal is related to the water content of the sample. The transverse relaxation time (T_2) of the mortar was measured using the Carr–Purcell–Meiboom–Gill (CPMG) pulse sequence, as expressed in Equation (1) [49].

$$\frac{1}{T_2} \approx \frac{1}{T_{2s}} = \rho\frac{S}{V} = \frac{\rho F_s}{R} = \frac{2\rho}{R} \quad (1)$$

where T_2s is the surface relaxation time and ρ is the surface relaxivity of T_2s, with ρ = 12 nm/ms [50]; S/V is the ratio of the pore surface area, S, to the fluid volume, V; R is the pore radius; and Fs is the pore geometry factor. In this study, the pore structure was assumed to be cylindrical, and Fs was therefore taken as 2.

3. Results

3.1. Setting Time and Compressive Strength

The setting times of the mortars with different mix proportions are shown in Figure 3a. With the incorporation of carbonated MSWI fly ash, both the initial and final setting times of the mortar were shortened. This can be attributed to the presence of calcite in the carbonated MSWI fly ash, which provided additional nucleation sites during hydration and thereby accelerated the setting process [5]. In contrast, the incorporation of hydrophobically modified MSWI fly ash prolonged the setting time of the mortar. This was because the hydrophobic groups in the fly ash hindered sufficient contact between cement and water, thus delaying cement hydration [51]. The compressive strengths of the mortars with different mix proportions are shown in Figure 3b. With the incorporation of carbonated MSWI fly ash, the compressive strength of the mortar increased. At 28 d, the compressive strength of the mortar containing carbonated MSWI fly ash increased by up to 4.5 MPa compared with that of the reference group. The incorporation of carbonated MSWI fly ash improved the compactness of the specimens, while also contributing to the immobilisation of heavy metals, resulting in more stable strength development [52]. Conversely, the compressive strength of the specimens gradually decreased with increasing incorporation of hydrophobically modified MSWI fly ash. At 28 d, the compressive strength of the mortar containing hydrophobically modified MSWI fly ash decreased by up to 9.7 MPa compared

with that of the reference group. This reduction was mainly attributed to the formation of low-surface-energy interfaces by hydrophobic groups within the mortar, which reduced the wetting and migration of water on the surfaces of particles and hydration products, thereby hindering the formation of a continuous and dense network of hydration products such as C–S–H [53]. In addition, interlayer water and confined water in C–S–H gel participate in hydrogen-bond networks and interparticle cohesion, and changes in their state may affect the structural stability and mechanical performance of the gel [54]. The strength of the specimens incorporating both hydrophobically modified and carbonated MSWI fly ash was higher than that of the specimens containing only hydrophobically modified MSWI fly ash, but lower than that of the specimens containing only carbonated MSWI fly ash. This indicates that the two modified materials exert balancing effects on the mechanical properties of mortar and can be used to regulate its strength development.

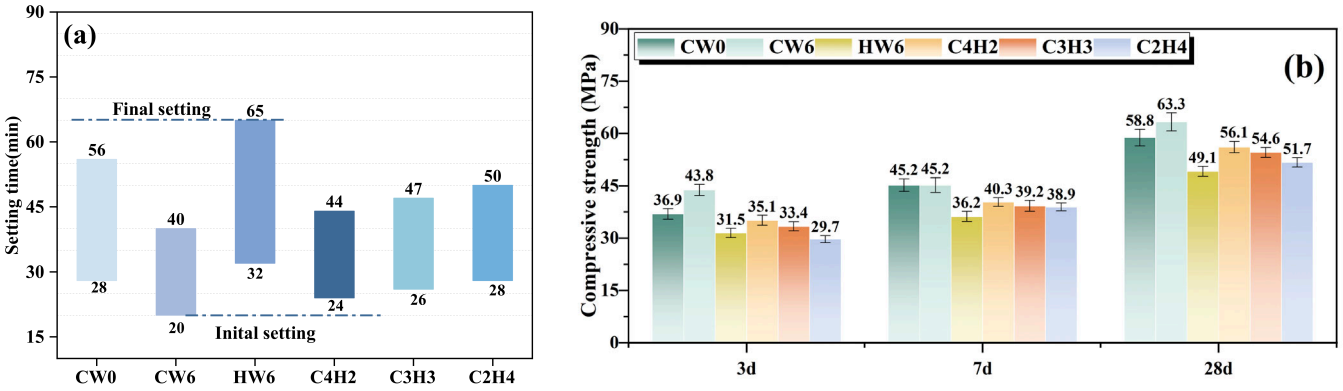

Figure 3. Properties of mortars with different mix proportions: (**a**) setting time; (**b**) compressive strength.

3.2. Heat of Hydration

The heat of hydration results of pastes with different mix proportions are shown in Figure 4. The different proportions of modified MSWI fly ash significantly affected the early-age hydration heat behaviour of the composite cementitious system. All specimens exhibited two distinct exothermic peaks. The first peak mainly corresponded to the initial wetting of cement particles, the rapid dissolution of ye'elimite, and the release of soluble components from fly ash, whereas the second peak was associated with the substantial formation of hydration products, such as AFt, AH_3, and C–S–H [55]. Compared with the co-modified specimens, the first and second peaks of the CW0 specimen appeared earliest. This may be attributed to the higher chloride content in the unmodified MSWI fly ash, as chlorides may promote early hydration and accelerate heat release. Among the co-modified specimens, C4H2 exhibited the highest cumulative heat release, reaching 114.88 J/g, indicating that a higher content of carbonated fly ash promoted hydration heat evolution. Carbonated MSWI fly ash can facilitate early hydration reactions through the nucleation effect of $CaCO_3$ [56]. With increasing replacement by hydrophobically modified MSWI fly ash, the cumulative heat release decreased to 111.29 J/g for C3H3 and 107.08 J/g for C2H4. This is because hydrophobically modified MSWI fly ash restricts water migration and ion diffusion, thereby inhibiting the hydration reaction of mortar; excessive hydrophobic components may weaken the promoting effect of carbonated fly ash [57]. Overall, carbonated MSWI fly ash mainly promotes heat release through $CaCO_3$ nucleation, pore filling, and the formation of hydration products, whereas hydrophobically modified MSWI fly ash suppresses the main hydration peak by reducing wettability and delaying water migration. Appropriate co-incorporation can regulate the hydration rate and hydration heat release.

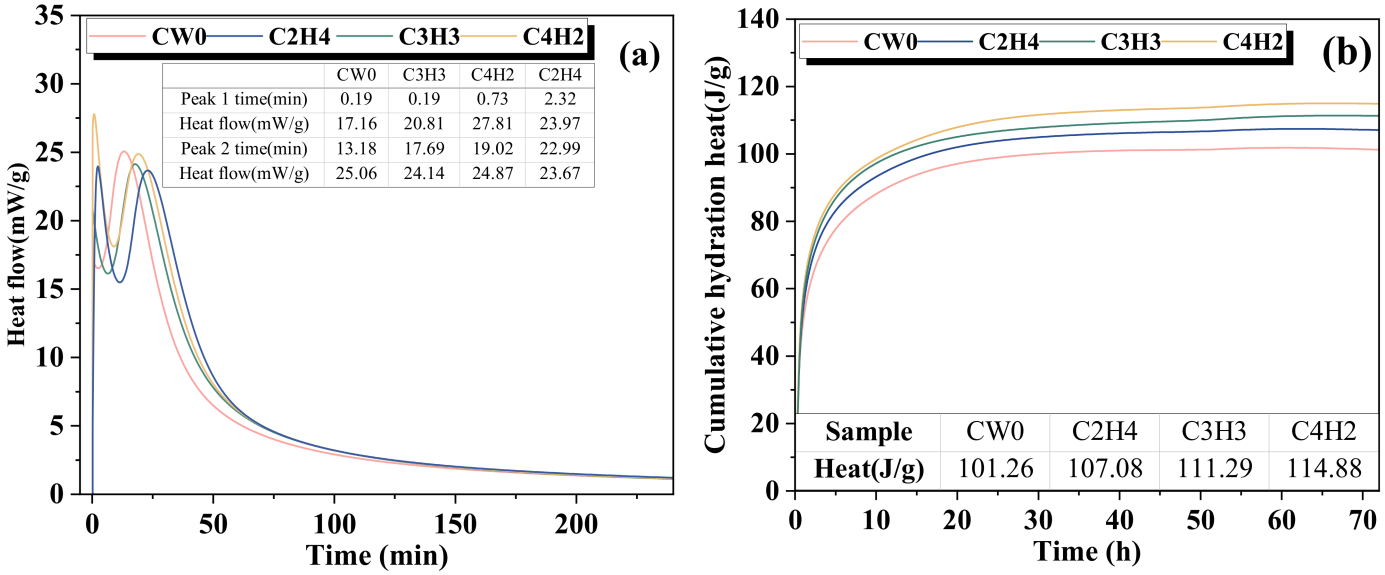

Figure 4. Heat of hydration of pastes with different mix proportions: (**a**) heat flow; (**b**) cumulative heat release.

3.3. Water Absorption and Electrically Accelerated Corrosion

The water absorption of mortars prepared with MSWI fly ash after curing for 28 d is shown in Figure 5. MSWI fly ash exhibits a loose, porous, and heterogeneous structure with a relatively high specific surface area, which endows it with strong water absorption capacity [33]. The water absorption process of mortar can be divided into a rapid water absorption stage, a transition stage, and a stable stage [58]. During the rapid water absorption stage, driven by the capillary suction of internal capillary pores, the water absorption of each mortar specimen reached approximately 90% of its total water absorption by around 8 h. With the incorporation of carbonated MSWI fly ash, the water absorption of the mortar decreased, with CW6 showing a reduction of 23.2%. Carbonated MSWI fly ash promoted the formation of C–S–H and $CaCO_3$ in the specimens, which filled pores and reduced pore connectivity, thereby weakening water migration and decreasing water absorption. With the incorporation of hydrophobically modified MSWI fly ash, the water absorption of the mortar also decreased, with HW6 showing a reduction of 33.4%. The silica in MSWI fly ash can bond with methylsiloxane hydrophobic groups and form a hydrophobic film within the pores of the matrix, thereby reducing water uptake [59]. When hydrophobically modified MSWI fly ash and carbonated MSWI fly ash were used together as replacements, the reduction in water absorption first increased and then decreased, with a maximum reduction of 39.9%. The synergistic incorporation of hydrophobically modified and carbonated MSWI fly ash at an appropriate ratio can balance the water absorption behaviour and compactness of mortar, further reducing the water absorption of the specimens [60].

The electrically accelerated corrosion morphologies of mortars with different mix proportions are shown in Figure 6. The reference specimen, CW0, exhibited obvious through-cracks on the surface, outward leakage of corrosion products, and interfacial deterioration around the steel bar. The mortar containing unmodified MSWI fly ash had relatively high contents of corrosive ions and high water absorption. Under the action of the electric field, water and corrosive ions migrated towards the steel–mortar interface, thereby accelerating the expansion of steel corrosion products and inducing cracking. After the incorporation of carbonated MSWI fly ash, the water absorption decreased from 6.52% for CW0 to 5.01% for CW6, and the corrosion cracks and rust staining showed a slight decreasing trend. This was mainly associated with the filling effect of carbonate products in the carbonated MSWI fly ash, which improved particle packing, refined some pores,

and reduced the connectivity of capillary water absorption channels, thereby delaying the ingress of corrosive media. However, local cracks and rust propagation were still observed in the CW specimens, indicating that carbonation treatment alone had a limited effect on water blocking and ion migration inhibition. The specimens incorporating hydrophobically modified MSWI fly ash exhibited lower water absorption. With the incorporation of hydrophobically modified MSWI fly ash, crack propagation and the outward leakage of corrosion products were weakened in the corrosion morphology. An appropriate amount of hydrophobic components could reduce the surface energy of pore walls, disrupt continuous water-film transport pathways, decrease the penetration of electrolyte solution into the steel–mortar interface, and thus improve corrosion resistance [61]. Among the co-modified specimens, C3H3 showed a water absorption of 3.92% and relatively slight corrosion damage, indicating a synergistic effect between suitable amounts of carbonated MSWI fly ash and hydrophobically modified MSWI fly ash. Carbonated MSWI fly ash reduced transport pathways through pore filling and matrix densification, whereas hydrophobically modified MSWI fly ash inhibited the migration of water and ions by forming a hydrophobic barrier. The reduction in water absorption was an important reason for the improvement in corrosion morphology. Overall, the water ingress resistance and corrosion resistance improvement induced by hydrophobically modified MSWI fly ash were superior to those achieved by carbonated MSWI fly ash alone, while the composite system exhibited a more favourable synergistic effect of pore filling and hydrophobic blocking. The water-absorption and electrically accelerated corrosion tests provide comparative, rather than long-term field, evidence. Lower water absorption and steel mass loss indicate reduced liquid and ion transport and improved corrosion-related performance under the adopted conditions.

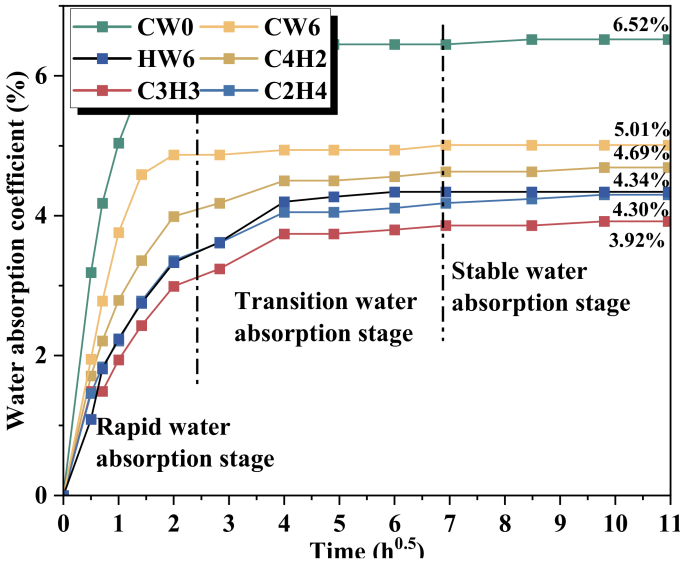

Figure 5. Water absorption of mortars with different mix proportions.

3.4. ICP-MS

The heavy-metal leaching results of the mortar specimens with different mix proportions are presented in Figure 7 and Table 3. The leaching concentrations of Cr, Cu, Zn, As, Cd, Pb, Mn, and Fe from the original MSWI fly ash were 11.9, 6.9, 29.1, 0.13, 0.36, 2.4, 10.0, and 172.5 mg/L, respectively. All regulated metals except Pb met the GB 18598—2019 [62] limits. The Pb concentration reached 2.4 mg/L, exceeding the limit of 1.2 mg/L, indicating a potential Pb-leaching risk and the need for modification and cement-based solidification to restrict its release. Compared with CW0, CW6, HW6, C4H2, and C2H4 further reduced the release concentrations of most metal elements, indicating that replacing unmodified fly ash

with modified MSWI fly ash can improve the environmental safety of the mortar system. Overall, the leaching concentrations of heavy metals in the mortar specimens with different mix proportions remained at relatively low levels, and the concentrations of Cr, Cu, Zn, As, Cd, and Pb were all below the limits specified in GB 18598—2019, demonstrating the effective immobilisation of heavy metals from MSWI fly ash in this system. Compared with the reference sample CW0, the incorporation of CWF, HWF, and their combined use reduced the concentrations of all heavy metals to varying degrees. Compared with CW0, CW6 reduced the leaching concentrations of Cr, Cu, Zn, As, Cd, and Pb by 39.3%, 29.4%, 13.0%, 25.0%, 50.0%, and 25.0%, respectively, with Cr, Cu, Cd, and Pb decreasing from 8.9, 1.7, 0.08, and 0.8 mg·L^{-1} to 5.4, 1.2, 0.04, and 0.6 mg/L, confirming that carbonation effectively suppressed heavy-metal release. This can be attributed to the reaction of alkaline components, such as CaO and $Ca(OH)_2$, with CO_2 during carbonation to form $CaCO_3$. This process not only reduced the content of free alkalis in fly ash, but also improved the compactness of the matrix through pore filling, adsorption, and encapsulation, thereby restricting the migration of some metal ions [5,56].

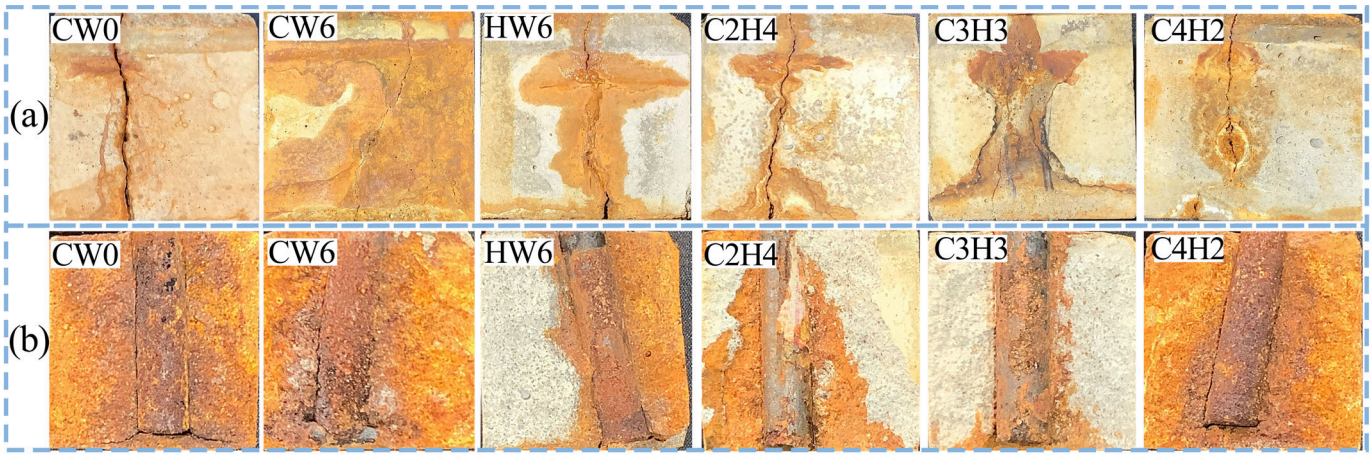

Figure 6. Electrically accelerated corrosion images of mortars with different mix proportions: (**a**) surface corrosion morphology; (**b**) steel–mortar interfacial corrosion morphology.

The hydrophobic-modified sample HW6 exhibited a more pronounced inhibitory effect on the release of certain elements. Compared with CW0, HW6 reduced the leaching concentrations of Cr, Cu, Zn, As, Cd, and Pb by 55.1%, 35.3%, 25.0%, 25.0%, 62.5%, and 37.5%, respectively, with Cr, Cu, Cd, and Pb decreasing to 4.0, 1.1, 0.03, and 0.5 mg/L. This indicates that hydrophobic-modified fly ash not only alters the surface wettability of particles, but also weakens capillary water absorption and ion migration pathways, thereby reducing the leaching of heavy metals from the mortar matrix by external solutions [59]. The combined modified samples C4H2 and C2H4 showed better stabilization effects. Compared with CW0, C2H4 reduced the leaching concentrations of Cr, Cu, Zn, As, Cd, and Pb by 57.3%, 47.1%, 36.0%, 50.0%, 50.0%, and 37.5%, respectively, with Cr, Cu, Zn, As, and Pb decreasing to 3.8, 0.9, 6.4, 0.02, and 0.5 mg/L and most elements reaching the lowest or near-lowest levels. These results suggest a synergistic effect between carbonation and hydrophobic modification. Carbonation products enhance heavy metal stability through pore filling and chemical solidification/stabilization, while hydrophobic components further block water transport pathways and reduce dissolution–diffusion migration processes, thereby jointly decreasing the leaching concentrations of heavy metals.

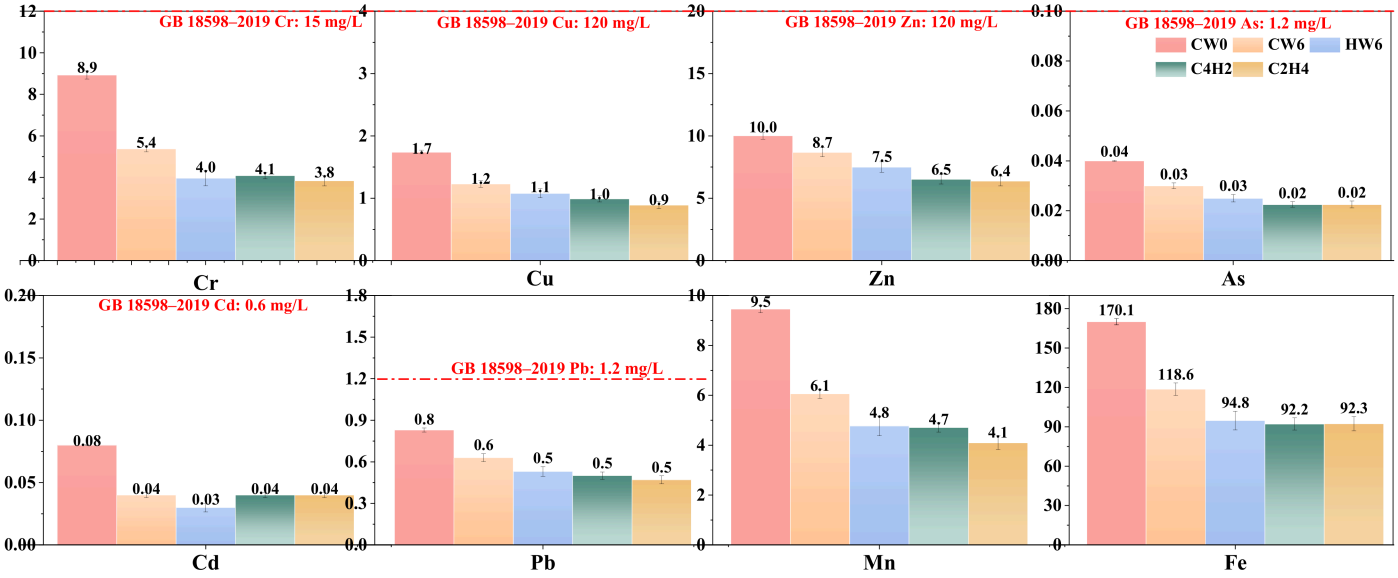

Figure 7. Heavy metal concentrations in mortar specimens with different mix proportions.

Table 3. Leaching concentrations of metal elements in the original MSWI fly ash and mortar specimens (mg/L).

Element	WF (mg·L^{-1})	CW0 (mg·L^{-1})	CW6 (mg·L^{-1}/%)	HW6 (mg·L^{-1}/%)	C4H2 (mg·L^{-1}/%)	C2H4 (mg·L^{-1}/%)	GB 18598—2019 Limit (mg·L^{-1})
Cr	11.9	8.9	5.4/39.3	4.0/55.1	4.1/53.9	3.8/57.3	15
Cu	6.9	1.7	1.2/29.4	1.1/35.3	1.0/41.2	0.9/47.1	120
Zn	29.1	10	8.7/13.0	7.5/25.0	6.5/35.0	6.4/36.0	120
As	0.13	0.04	0.03/25.0	0.03/25.0	0.02/50.0	0.02/50.0	1.2
Cd	0.36	0.08	0.04/50.0	0.03/62.5	0.04/50.0	0.04/50.0	0.6
Pb	2.4	0.8	0.6/25.0	0.5/37.5	0.5/37.5	0.5/37.5	1.2
Mn	10	9.5	6.1/35.8	4.8/49.5	4.7/50.5	4.1/56.8	—
Fe	172.5	170.1	118.6/30.3	94.8/44.3	92.2/45.8	92.3/45.7	—

Note: Values after "/" represent the percentage reduction in leaching concentration relative to CW0, calculated as ($R = \frac{C_{CW0} - C_i}{C_{CW0}} \times 100\%$). "—" indicates that no corresponding limit was specified.

3.5. XRD

The XRD patterns of the mortars prepared with different mix proportions are shown in Figure 8. The crystalline phases identified in the mortar specimens included SiO_2, $CaCO_3$, $CaSO_4$, $Ca(OH)_2$, AFt, C_2S, C_4A_3S, C_4ACH_{11}, and Friedel's salt [63,64]. The diffraction peak at approximately 26.7° was mainly assigned to SiO_2 (quartz), originating primarily from the quartz sand and unreacted siliceous components. Variations in its intensity may be attributed to the non-uniform local distribution of sand particles. A $CaCO_3$ peak was observed at approximately 29°, suggesting the presence of a distinct carbonate phase in the system. The peaks at 31–35°, around 39°, and several low-intensity peaks were assigned to AFt, Friedel's salt, and sulphoaluminate hydration products, indicating that Cl^-, SO_4^{2-}, Ca, and Al components in the fly ash participated in hydration reconstruction and immobilisation reactions [65].

Friedel's salt and AFt were detected in the mortars, which can be attributed to the ability of calcium aluminates in sulfoaluminate cement to bind Cl^- and SO_4^{2-}, leading to the formation of Friedel's salt and AFt [65]. Compared with CW0, the diffraction peaks of $CaCO_3$ and calcium carboaluminate hydrates became more distinct in CW6 with the incorporation of carbonated MSWI fly ash. This is because the carbonated fly ash introduced pre-formed $CaCO_3$ into the system, and $CaCO_3$ could react with C_4A_3S in the

cement and $Ca(OH)_2$ in the hydration products to form calcium carboaluminate hydrates, such as C_4ACH_{11} [66,67]. In addition, the preparation of carbonated MSWI fly ash involved a washing step, which reduced its internal chloride content. As a result, the content of Friedel's salt in CW6 decreased. The variations in AFt and Friedel's salt in HW6 were similar to those observed in CW6. Moreover, a relatively strong $Ca(OH)_2$ peak was observed in the hydrophobic-modified MSWI fly ash sample. Hydrophobic-modified fly ash inhibited the rapid dissolution of salts and reactive components within the fly ash, so the consumption of calcium hydroxide was less pronounced than that in highly reactive systems. The C4H2, C3H3, and C2H4 samples exhibited both the carbonate stabilization effect of carbonated fly ash and the transport-regulating effect of hydrophobic-modified fly ash. Specifically, carbonated fly ash provided a stable carbonate framework and improved the pore structure, whereas hydrophobic-modified fly ash reduced continuous water transport. Together with the fixation of Cl^- by Friedel's salt, this contributed to suppressing the diffusion of aggressive media.

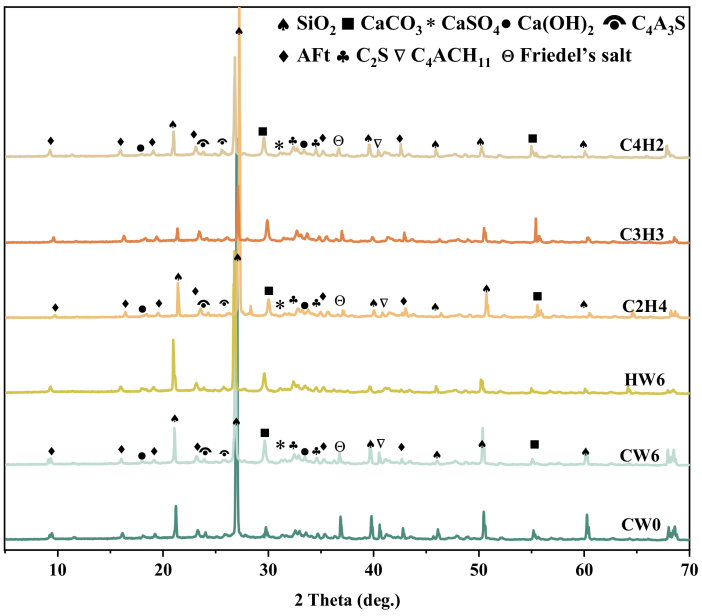

Figure 8. XRD patterns of mortars with different mix proportions.

3.6. FTIR

The FTIR spectra of mortars prepared with different proportions of MSWI fly ash are shown in Figure 9. The broad band observed at approximately 3628–3426 cm^{-1} can be attributed to the vibrations of H_2O and OH^-, while the band at 1650 cm^{-1} corresponds to the H–O–H bending vibration, indicating the presence of adsorbed or bound water to varying degrees in all specimens. The absorption band near 1109 cm^{-1} is associated with SO_4^{2-}, whereas the bands around 796, 740, 525, and 470 cm^{-1} are mainly related to Si–O vibrations [33,64]. Compared with CW0, the characteristic CO_3^{2-} peaks of the CW6 specimen near 1420 cm^{-1} and 870 cm^{-1} were markedly enhanced, indicating that Ca-based reactive components and some hydration products were further converted into carbonate phases after carbonation, indicating stronger carbonate-related signals in CW6. Carbonation not only increased the carbonate content, but also consumed the original alkaline Ca phases to some extent, resulting in smoother OH^- and H_2O peak profiles and reflecting the characteristics of dealkalisation carbonation. HW6 mainly exhibited the introduction of organic hydrophobic groups. The absorption peaks near 2918 cm^{-1} and 2850 cm^{-1} can be assigned to the stretching vibrations of alkyl C–H bonds, indicating that the organic groups from the hydrophobic modifier were successfully introduced into

the mortar [68]. C2H4, C3H3, and C4H2 exhibited the dual characteristics of carbonation and hydrophobic modification. On the one hand, the CO_3^{2-} peaks near 1420 cm^{-1} and 870 cm^{-1} indicated the presence of distinct carbonation products in the system; on the other hand, organic group absorption peaks similar to those of the hydrophobically modified group were still observed, supporting the coexistence of hydrophobic functional groups and carbonate-related products in the synergistically modified system.

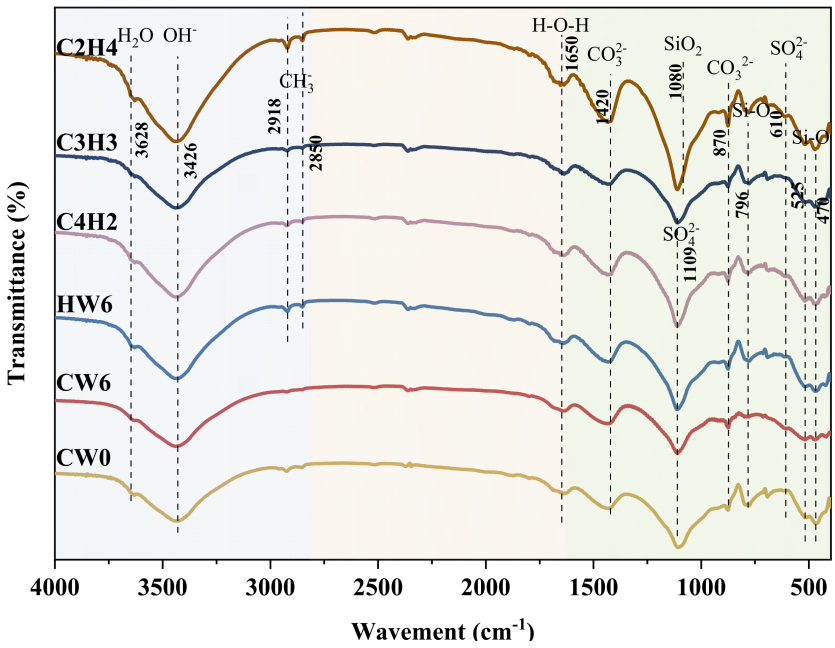

Figure 9. FTIR spectra of mortars with different mix proportions.

3.7. NMR

The NMR results of mortars with different mix proportions are shown in Figure 10. CW0 exhibited the highest porosity of 6.27%, indicating that unmodified MSWI fly ash led to the formation of more pores within the mortar matrix. This can be attributed to the loose and porous structure, high water absorption, and high chloride content of raw fly ash, which tend to increase the water demand of the paste and result in a less compact microstructure [69]. Compared with CW0, the porosity of CW6 decreased to 5.75%. Carbonation treatment reduced the micropore volume, refined the pore size, and improved the compactness of the matrix through $CaCO_3$ precipitation covering and filling the surface and internal pores of fly ash particles [70]. In terms of pore size distribution, CW0 showed the highest peak intensity in the dominant peak region, accompanied by a distinct tail in the macropore region, suggesting that it had not only a higher total porosity but also a broader pore structure. After the incorporation of carbonated MSWI fly ash, the main peak of CW6 decreased significantly, indicating that the dominant pore population was effectively compressed. As shown in Figure 10c, the proportion of pores sized 20–50 nm in CW6 decreased from 2.24% in CW0 to 2.02%, while pores sized 50–100 nm decreased from 0.56% to 0.35%, and pores larger than 100 nm decreased from 0.59% to 0.38%. These results demonstrate that carbonation was particularly effective in reducing medium-sized pores and larger harmful pores, directly reflecting the pore-filling and pore-blocking effects of $CaCO_3$.

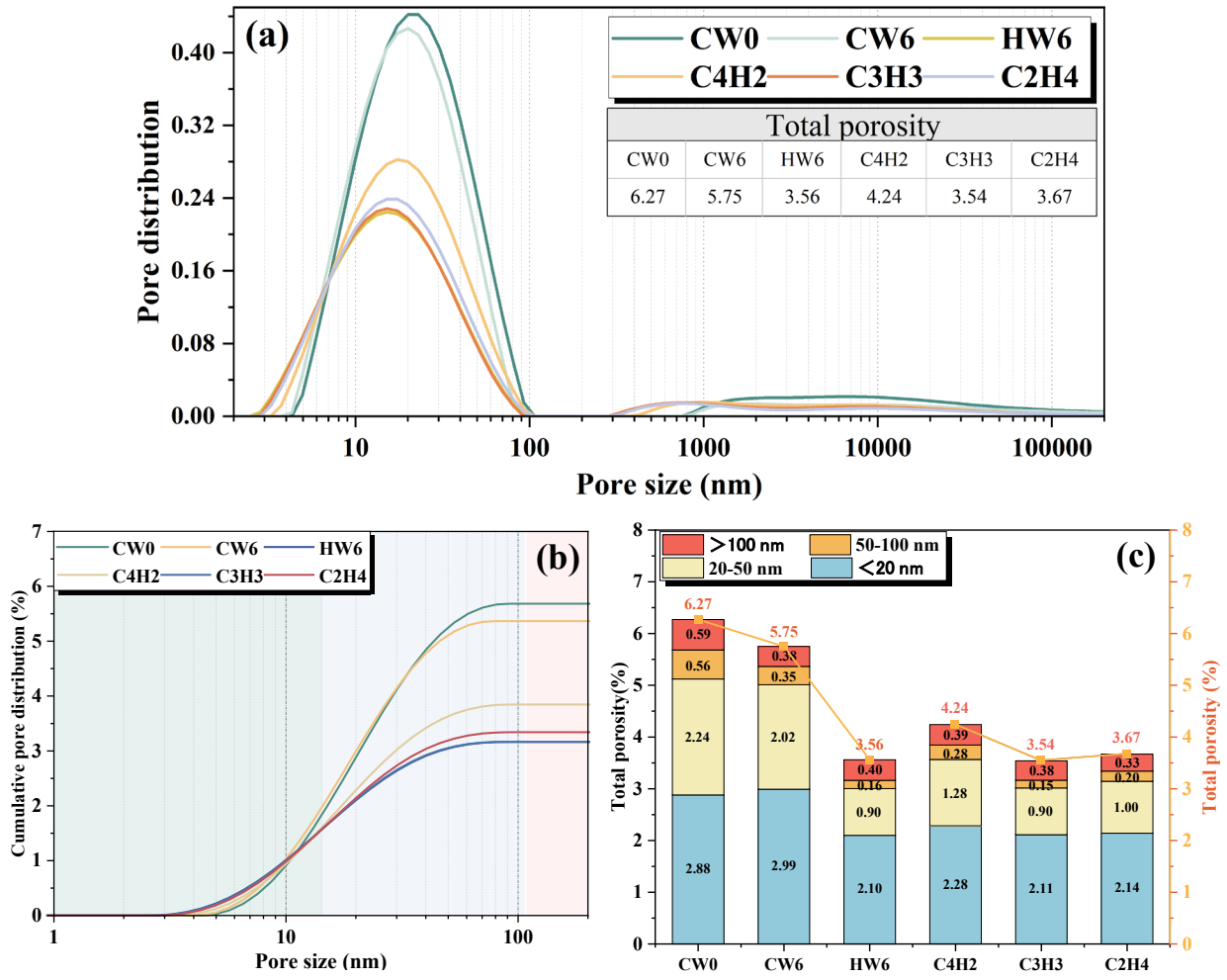

Figure 10. Pore characteristics of mortars with different mix proportions: (**a**) pore-size frequency distribution; (**b**) cumulative pore-size distribution; and (**c**) pore distribution in different size ranges and total porosity.

The total porosity of HW6 was 3.56%, which was lower than that of CW6. The proportion of pores sized 20–50 nm decreased from 2.24% in CW0 to 0.90%, while pores larger than 100 nm decreased to approximately 0.40%. This indicates that hydrophobic treatment not only inhibited the development of mesopores into connected capillary pores, but also effectively reduced large pores and potential crack-like pores. Hydrophobic modification lowered the surface free energy of reaction products and pore walls and weakened the continuous transport of water within the pore channels, thereby disrupting the connected capillary pore network that would otherwise readily form [71]. The total porosities of the combined-modified samples C4H2, C3H3, and C2H4 were 4.24%, 3.54%, and 3.67%, respectively, with C3H3 showing the lowest value. The synergistic modification did not rely on maximizing the replacement level of either single treatment, but rather on balancing the two mechanisms. In the C3H3 mixture, the $CaCO_3$ filling and pore refinement provided by carbonated fly ash were more effectively coupled with the water-repellent and connected-pore-blocking effects of hydrophobic-modified fly ash. As shown in Figure 10c, C3H3 exhibited relatively low proportions in all four pore categories, indicating not only a lower total porosity but also a more effective suppression of harmful pores and a more balanced pore structure. Therefore, in the synergistic system, carbonation mainly contributed to pore filling and mineral reconstruction, whereas hydrophobic modification weakened liquid water connectivity and subsequent pore development. When

these two effects were properly matched, both the total porosity and the proportion of harmful pores were simultaneously reduced.

3.8. TG

The TG curves of the different mortar specimens are shown in Figure 11, and the mass losses at different stages are listed in Table 4. The mass loss at 40–105 °C (W_0) was mainly associated with the removal of free water and some bound water, accompanied by the dehydration of hydration products such as AFt and C–S–H [72]. The mass loss at 105–400 °C (W_I) mainly corresponded to the decomposition of $CaSO_4 \cdot 2H_2O$, AFm, and $Al(OH)_3$ [73,74]. The mass loss at 400–600 °C (W_{II}) was mainly attributed to the decomposition of $Ca(OH)_2$ [75], while the mass loss at 600–800 °C (W_{III}) was assigned to the decarbonation decomposition of $CaCO_3$ [76].

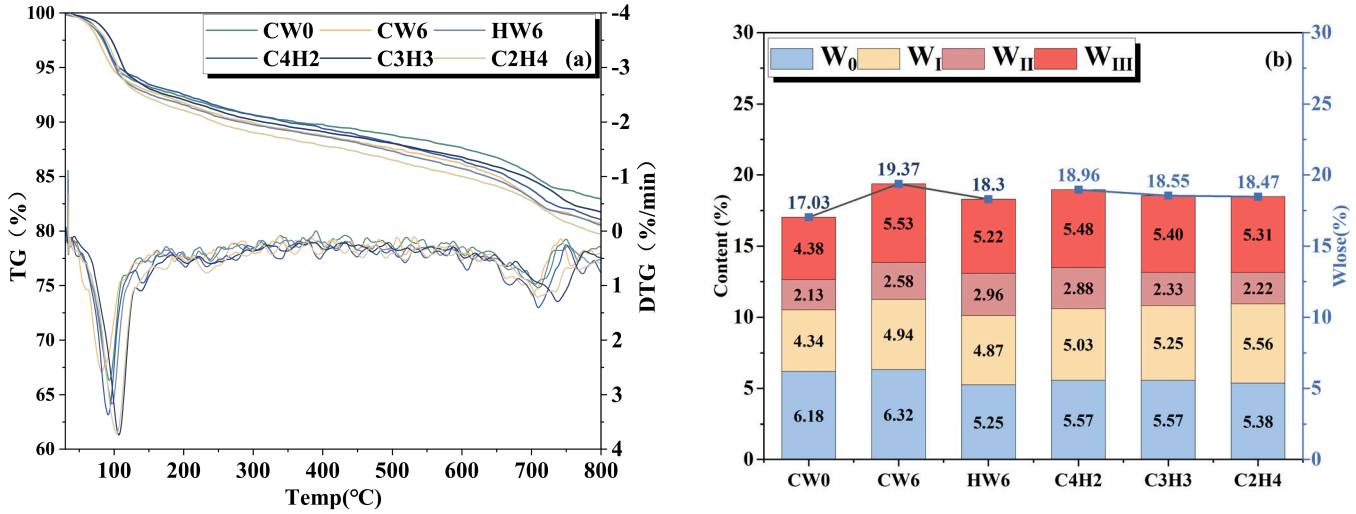

Figure 11. TG analysis results of mortars with different mix proportions: (**a**) TG–DTG curves; (**b**) mass loss in different temperature ranges and total mass loss.

Table 4. Related data of mass loss at different heating stages (wt%).

Samples	W_0	W_I	W_{II}	W_{III}	W_{lose}
CW0	6.18	4.34	2.13	4.38	17.03
CW6	6.32	4.94	2.58	5.53	19.37
HW6	5.25	4.87	2.96	5.22	18.30
C4H2	5.57	5.03	2.88	5.48	18.96
C3H3	5.57	5.25	2.33	5.40	18.55
C2H4	5.38	5.56	2.22	5.31	18.47

Compared with CW0, the incorporation of carbonated MSWI fly ash increased the total mass loss of CW6 to 19.37%, indicating an overall increase in thermally decomposable components. Specifically, W_I increased from 4.34% to 4.94%, W_{II} from 2.13% to 2.58%, and W_{III} from 4.38% to 5.53%. These results suggest that carbonated MSWI fly ash promoted the hydration degree of the samples, induced the formation of more carbonate phases, and facilitated the accumulation of hydration products in the low- and medium-temperature ranges. The incorporation of hydrophobic-modified MSWI fly ash also increased the total mass loss, with HW6 showing a W_{lose} value of 19.30%. Meanwhile, the W_0 content decreased markedly, indicating that hydrophobic-modified MSWI fly ash reduced the moisture content of the samples and inhibited the formation of some hydration products. The combined replacement samples reflected the synergistic effect between carbonated

and hydrophobic-modified MSWI fly ash. The total mass losses of the three combined-modified samples were all higher than that of CW0, and their W_I, W_{II}, and W_{III} values increased, suggesting that combined modification favored the accumulation of hydration products. Among them, C4H2 exhibited a W_{lose} value of 18.96%, and its W_{III} reached 5.48%, indicating that a higher proportion of carbonated fly ash increased the carbonate content in the combined system. With increasing hydrophobic-modified MSWI fly ash content, the free water content decreased and the amount of hydration products was slightly reduced. However, the mass loss of C3H3 at each stage remained at an intermediate level, showing relatively balanced but not prominent thermal decomposition characteristics.

4. Conclusions

This study investigated the combined use of carbonated and hydrophobically modified MSWI fly ashes in mortar. The principal conclusions are as follows:

(1) Carbonation and hydrophobic modification produced complementary but competing effects. Carbonated MSWI fly ash promoted early hydration, strength development, and carbonate-related pore filling, whereas hydrophobically modified fly ash reduced particle wettability and water transport but partially delayed hydration and weakened strength development. Their combined use therefore provided a means of balancing mechanical performance, moisture resistance, and environmental stability rather than maximising a single property.

(2) No single mixture exhibited the best performance in all respects. Within the investigated range, C3H3 provided the most balanced engineering performance, showing relatively low water absorption, limited visible corrosion damage, and the lowest measured porosity. By contrast, C2H4 generally exhibited the greatest reductions in the leaching of several metal elements. The proportion of carbonated and hydrophobically modified fly ashes should therefore be selected according to the intended performance requirement.

(3) The combined XRD, FTIR, TG, and NMR results were consistent with a mechanism involving carbonate-related pore filling and hydrophobic blocking of liquid and ion transport. However, these results mainly provide qualitative or comparative evidence and do not constitute definitive quantitative phase analysis. The observed reductions in water absorption, accelerated corrosion damage, and heavy-metal leaching should likewise be interpreted as relative improvements under the adopted laboratory conditions.

(4) The proposed approach shows potential for producing MSWI fly ash-containing mortars requiring reduced water uptake and controlled contaminant release. Nevertheless, the present study was limited to six mixtures at a fixed total fly ash dosage, short-term water-absorption, electrically accelerated corrosion, and laboratory leaching tests. Long-term chloride migration, sorptivity, surface resistivity, cyclic leaching, natural exposure, and quantitative phase analysis are required before field durability and large-scale application can be established.

Author Contributions: Conceptualization, J.Z. and J.L.; methodology, Y.Z.; software, K.Z.; validation, J.Z., Y.Z. and K.Z.; formal analysis, K.Z.; investigation, K.Z.; resources, Y.Z.; data curation, Y.Z.; writing—original draft preparation, Y.Z. and K.Z.; writing—review and editing, Y.Z.; visualization, J.L.; supervision, J.L.; project administration, J.Z.; funding acquisition, J.Z. All authors have read and agreed to the published version of the manuscript.

Funding: This work was supported by the National Natural Science Foundation of China (52578444), the Key Research and Development Special Program of Henan Province (241111322500) and the Support Plan for University Science and Technology Innovation Team of Henan Province (24IRTSTHN009).

Data Availability Statement: Data are contained within the article.

Acknowledgments: The authors would like to thank the laboratory staff for their technical support during the experimental testing and sample characterization.

Conflicts of Interest: The authors declare no conflicts of interest.

References

1. Chen, L.; Wang, L.; Cho, D.-W.; Tsang, D.C.W.; Tong, L.; Zhou, Y.; Yang, J.; Hu, Q.; Poon, C.S. Sustainable stabilization/solidification of municipal solid waste incinerator fly ash by incorporation of green materials. *J. Clean. Prod.* **2019**, *222*, 335–343. [CrossRef]
2. Wang, B.; Chen, Q.; Yun, M.; Huang, J.; Sun, J. Development of a comprehensive pollution evaluation system based on entropy weight-fuzzy evaluation model for urban rivers: A case study in North China. *J. Water Process Eng.* **2024**, *67*, 106192. [CrossRef]
3. Kundariya, N.; Mohanty, S.S.; Varjani, S.; Hao Ngo, H.; Wong, J.W.C.; Taherzadeh, M.J.; Chang, J.-S.; Yong Ng, H.; Kim, S.-H.; Bui, X.-T. A review on integrated approaches for municipal solid waste for environmental and economical relevance: Monitoring tools, technologies, and strategic innovations. *Bioresour. Technol.* **2021**, *342*, 125982. [CrossRef] [PubMed]
4. Yakubu, Y.; Zhou, J.; Ping, D.; Shu, Z.; Chen, Y. Effects of pH dynamics on solidification/stabilization of municipal solid waste incineration fly ash. *J. Environ. Manag.* **2018**, *207*, 243–248. [CrossRef] [PubMed]
5. Chen, T.-L.; Chen, Y.-H.; Dai, M.-Y.; Chiang, P.-C. Stabilization-solidification-utilization of MSWI fly ash coupling CO_2 mineralization using a high-gravity rotating packed bed. *Waste Manag.* **2021**, *121*, 412–421. [CrossRef] [PubMed]
6. Ministry of Ecology and Environment of the People's Republic of China. *Compilation Explanation for the Technical Specification for Pollution Control of Construction Waste (Draft for Comments)*; Ministry of Ecology and Environment of the People's Republic of China: Beijing, China, 2025.
7. Ministry of Ecology and Environment of the People's Republic of China. *Report on the State of the Ecology and Environment in China 2024*; Ministry of Ecology and Environment of the People's Republic of China: Beijing, China, 2025.
8. Li, X.; Sun, Y.; Li, W.; Nie, Y.; Wang, F.; Bian, R.; Wang, H.; Wang, Y.-n.; Gong, Z.; Lu, J.; et al. Solidification/stabilization pre-treatment coupled with landfill disposal of heavy metals in MSWI fly ash in China: A systematic review. *J. Hazard. Mater.* **2024**, *478*, 135479. [CrossRef] [PubMed]
9. Clavier, K.A.; Liu, Y.; Intrakamhaeng, V.; Townsend, T.G. Re-evaluating the TCLP's Role as the Regulatory Driver in the Management of Municipal Solid Waste Incinerator Ash. *Environ. Sci. Technol.* **2019**, *53*, 7964–7973. [CrossRef] [PubMed]
10. Chiang, K.-Y.; Hu, Y.-H. Water washing effects on metals emission reduction during municipal solid waste incinerator (MSWI) fly ash melting process. *Waste Manag.* **2010**, *30*, 831–838. [CrossRef] [PubMed]
11. Shunda, l.; Jiang, X.; Zhao, Y.; Yan, J. Disposal technology and new progress for dioxins and heavy metals in fly ash from municipal solid waste incineration: A critical review. *Environ. Pollut.* **2022**, *311*, 119878. [CrossRef] [PubMed]
12. Qi, C.; Zhang, R.; Zhou, W.; Zhang, T.; Zhang, X.; Bai, J.; Zhao, Y.; Bian, B. New model of municipal solid waste incineration fly ash treatment and its comprehensive benefits. *Waste Manag.* **2026**, *212*, 115318. [CrossRef] [PubMed]
13. Li, A.; Huang, C.; Feng, X.; Li, Y.; Yang, H.; Wang, S.; Li, J. Upgradation of sludge deep dewatering conditioners through persulfate activated by ferrous: Compatibility with sludge incineration, dewatering mechanism, ecological risks elimination and carbon emission performance. *Environ. Res.* **2022**, *211*, 113024. [CrossRef] [PubMed]
14. Chen, B.; Ye, G. The role of water-treated municipal solid waste incineration (MSWI) bottom ash in microstructure formation and strength development of blended cement pastes. *Cem. Concr. Res.* **2024**, *178*, 107440. [CrossRef]
15. Abbas, Z.; Moghaddam, A.P.; Steenari, B.-M. Release of salts from municipal solid waste combustion residues. *Waste Manag.* **2003**, *23*, 291–305. [CrossRef] [PubMed]
16. Kirkelund, G.M.; Jensen, P.E. Electrodialytic treatment of Greenlandic municipal solid waste incineration fly ash. *Waste Manag.* **2018**, *80*, 241–251. [CrossRef] [PubMed]
17. Fan, Y.; Li, Z.; Liu, L.; Xi, J. Combination of liquid-phase pulsed discharge and ultrasonic for saponins extraction from lychee seeds. *Ultrason. Sonochem.* **2020**, *69*, 105264. [CrossRef] [PubMed]
18. Fang, S.; Xu, L.; Wu, H.; Xu, Y.; Wang, Z.; Shu, K.; Hu, Y. Influence of surface dissolution on sodium oleate adsorption on ilmenite and its gangue minerals by ultrasonic treatment. *Appl. Surf. Sci.* **2020**, *500*, 144038. [CrossRef]
19. Kiani, A.; Acocella, M.R.; Granata, V.; Mazzotta, E.; Malitesta, C.; Guerra, G. Green Oxidation of Carbon Black by Dry Ball Milling. *ACS Sustain. Chem. Eng.* **2022**, *10*, 16019–16026. [CrossRef]
20. Jin, L.; Chen, M.; Wang, Y.; Peng, Y.; Yao, Q.; Ding, J.; Ma, B.; Lu, S. Utilization of mechanochemically pretreated municipal solid waste incineration fly ash for supplementary cementitious material. *J. Environ. Chem. Eng.* **2023**, *11*, 109112. [CrossRef]
21. Li, H.; Peng, Y.; Xu, M.; Wang, Y.; Ding, J.; Ma, B.; Jin, L.; Lu, S.; Yan, J. Use of municipal solid waste incineration fly ash as a supplementary cementitious material: CO_2 mineralization coupled with mechanochemical pretreatment. *Environ. Res.* **2024**, *242*, 117799. [CrossRef] [PubMed]

22. Wang, X.; Zhang, L.; Zhu, K.; Li, C.; Zhang, Y.; Li, A. Distribution and chemical species transition behavior of chlorides in municipal solid waste incineration fly ash during the pressure-assisted sintering treatment. *Chem. Eng. J.* **2021**, *415*, 128873. [CrossRef]
23. Ma, X.; Li, X.; Cao, R.; Su, F.; Yang, R.; Gao, C. Modification and detoxification of high-temperature sintering fluidized bed incineration fly ash and its performance as the cement admixture. *Constr. Build. Mater.* **2025**, *503*, 144588. [CrossRef]
24. You, K.-s.; Ahn, J.-W. Performance of sintering process to synthesize cementitious materials and to stabilize heavy metals from MSWI fly ash and water sludge. *Geosyst. Eng.* **2012**, *15*, 261–268. [CrossRef]
25. Hou, X.; Li, J.; Guan, C.; Zhang, X.; Wang, X.; Li, Y.; Li, Y.; Shi, W.; Wang, W. Effect of carbonization on chloride penetration in rapid repair mortar derived from solid waste-based CSA cement. *Case Stud. Constr. Mater.* **2025**, *23*, e04956. [CrossRef]
26. Gao, F.; Ge, Z.; Zhang, S.; Fang, H.; Zhang, H.; Shao, Y.; Lyu, J.; Zhang, H. Influence of carbonized fly ash on the early-age shrinkage of blended cement paste with different water-to-binder ratios. *Case Stud. Constr. Mater.* **2025**, *22*, e04607. [CrossRef]
27. Sun, Y.; Tao, Y.; Li, Z.; Lu, W.; Liu, Z.; Zhai, S.; Zhang, J. Accelerated carbonation of MSWI fly ash as a supplementary precursor in alkali-activated materials. *Dev. Built Environ.* **2025**, *22*, 100651. [CrossRef]
28. Li, S.; Chen, Y.; Wei, W.; Fang, G.; Duan, W. The increase in extreme precipitation and its proportion over global land. *J. Hydrol.* **2024**, *628*, 130456. [CrossRef]
29. Guccione, A.; Bassi, P.; Desbiolles, F.; Borgnino, M.; D'Andrea, F.; Pasquero, C. Extreme precipitation changes in relation to urbanization. *npj Nat. Hazards* **2026**, *3*, 10. [CrossRef]
30. Harilal, M.; Kamde, D.K.; Uthaman, S.; George, R.P.; Pillai, R.G.; Philip, J.; Albert, S.K. The chloride-induced corrosion of a fly ash concrete with nanoparticles and corrosion inhibitor. *Constr. Build. Mater.* **2021**, *274*, 122097. [CrossRef]
31. Huang, B.; Gan, M.; Ji, Z.; Fan, X.; Zhang, D.; Chen, X.; Sun, Z.; Huang, X.; Fan, Y. Recent progress on the thermal treatment and resource utilization technologies of municipal waste incineration fly ash: A review. *Process Saf. Environ. Prot.* **2022**, *159*, 547–565. [CrossRef]
32. Wang, X.; Li, A.; Zhang, Z. The Effects of Water Washing on Cement-based Stabilization of MWSI Fly Ash. *Procedia Environ. Sci.* **2016**, *31*, 440–446. [CrossRef]
33. Su, L.; Li, S.; Wu, S.; Liang, B.; Zhang, X. Preparation and heavy metal solidification mechanism of physically activated municipal solid waste incineration fly ash base geopolymer backfill. *Process Saf. Environ. Prot.* **2025**, *201*, 107522. [CrossRef]
34. Zhang, C.; Zhang, S.; Yu, J.; Kong, X. Water absorption behavior of hydrophobized concrete using silane emulsion as admixture. *Cem. Concr. Res.* **2022**, *154*, 106738. [CrossRef]
35. Song, J.; Zhao, D.; Han, Z.; Xu, W.; Lu, Y.; Liu, X.; Liu, B.; Carmalt, C.J.; Deng, X.; Parkin, I.P. Super-robust superhydrophobic concrete. *J. Mater. Chem. A* **2017**, *5*, 14542–14550. [CrossRef]
36. Ogawa, N.; Amano, T.; Nagai, Y.; Hagiwara, K.; Honda, T.; Koike, Y. Water repellents for the leaching control of heavy metals in municipal solid waste incineration fly ash. *Waste Manag.* **2021**, *124*, 154–159. [CrossRef] [PubMed]
37. Atanes, E.; Cuesta-García, B.; Nieto-Márquez, A.; Fernández-Martínez, F. A mixed separation-immobilization method for soluble salts removal and stabilization of heavy metals in municipal solid waste incineration fly ash. *J. Environ. Manag.* **2019**, *240*, 359–367. [CrossRef] [PubMed]
38. Chen, W.; Kirkelund, G.M.; Jensen, P.E.; Ottosen, L.M. Comparison of different MSWI fly ash treatment processes on the thermal behavior of As, Cr, Pb and Zn in the ash. *Waste Manag.* **2017**, *68*, 240–251. [CrossRef] [PubMed]
39. Wi, K.; Sahin, O.; Wang, K.; Lee, Y. Characterization and evaluation of cement-based systems containing solution-treated municipal solid-waste incineration fly ash. *Constr. Build. Mater.* **2024**, *416*, 135230. [CrossRef]
40. Abdi, E.; Asadollahfardi, G.; Salehi, A.; Akbardoost, J.; Esmaeili, N.; Panahandeh, A. Using Municipal Solid-Waste Incinerator Fly Ash, Wash Water, and Propylene Fibers in Self-Compacting Repair Mortar, Greenhouse Gas Emissions Potential. *Int. J. Concr. Struct. Mater.* **2024**, *18*, 57. [CrossRef]
41. Poranek, N.; Pizoń, J.; Łaźniewska-Piekarczyk, B.; Czajkowski, A.; Lagashkin, R. Recycle Option for Municipal Solid Waste Incineration Fly Ash (MSWIFA) as a Partial Replacement for Cement in Mortars Containing Calcium Sulfoaluminate Cement (CSA) and Portland Cement to Save the Environment and Natural Resources. *Materials* **2023**, *17*, 39. [CrossRef] [PubMed]
42. *GB/T 17671-2021*; Inspection Method for Strength of Cement (ISO Method). China Architecture and Building Press: Beijing, China, 2021. (In Chinese)
43. *GB/T 1346-2024*; Test Methods for Water Requirement of Standard Consistency, Setting Time and Soundness of the Portland Cement. China Standard Press: Beijing, China, 2024. (In Chinese)
44. Usherov-Marshak, A.V.V.; Ciak, M.J. Isothermal calorimetry in the standard ASTM C1679-08. *Cem. Wapno Beton* **2010**, *15*, 108–110.
45. *GB/T 50081-2019*; Standard for Test Methods of Concrete Physical and Mechanical Properties. China Construction Industry Press: Beijing, China; People's Republic of China and Ministry of Urban and Rural Construction: Beijing, China, 2019.
46. Liang, J.; Zhu, H.; Chen, L.; Han, X.; Guo, Q.; Gao, Y.; Liu, C. Rebar corrosion investigation in rubber aggregate concrete via the chloride electro-accelerated test. *Materials* **2019**, *12*, 862. [CrossRef] [PubMed]

47. Han, J.; Miao, Z.; Wang, J.; Zhang, X.; Lv, Y. Investigation of the corrosion-induced damage mechanism of steel fibers in ultra-high-performance steel fiber-reinforced concrete using X-ray computed tomography. *Constr. Build. Mater.* **2023**, *368*, 130429. [CrossRef]
48. Xue, J.; Wang, W.; Wang, Q.; Liu, S.; Yang, J.; Wui, T. Removal of heavy metals from municipal solid waste incineration (MSWI) fly ash by traditional and microwave acid extraction. *J. Chem. Technol. Biotechnol.* **2010**, *85*, 1268–1277. [CrossRef]
49. Shen, M.; Zhao, Y.; Bi, J.; Wang, C.; Ning, L.; Deng, X.; Zhang, K.; Du, B. Micro-damage evolution and macro-mechanical property of preloaded sandstone subjected to high-temperature treatment based on NMR technique. *Constr. Build. Mater.* **2023**, *369*, 130638. [CrossRef]
50. Ning, L.; Zhao, Y.; Bi, J.; Wang, C.; Shen, M.; Li, Y. Effect of aggregate size on water distribution and pore fractal characteristics during hydration of cement mortar based on low-field NMR technology. *Constr. Build. Mater.* **2023**, *389*, 131670. [CrossRef]
51. Ruan, S.; Chen, S.; Liu, Y.; Zhang, Y.; Yan, D.; Zhang, M. Early-age deformation of hydrophobized metakaolin-based geopolymers. *Cem. Concr. Res.* **2023**, *169*, 107168. [CrossRef]
52. Liang, D.; Li, M.; Yan, J.; Xu, C.; He, F.; Yang, W.; Xu, Y.; Wang, F.; Xue, S.; Lv, G.; et al. Effect and mechanism of CO_2 mineralization on the performance of geopolymer from municipal solid waste incineration fly ash. *Constr. Build. Mater.* **2025**, *485*, 141939. [CrossRef]
53. Chen, B.; Wang, M.; Manzano, H.; Zhao, Y.; Li, Y. Molecular elucidation of cement hydration inhibition by silane coupling agents. *Nat. Commun.* **2025**, *16*, 1597. [CrossRef] [PubMed]
54. Guo, J.; Liu, Q.; Zhang, Y.; Lu, W.; Li, D. Pore water effects on the structure, bonding, dynamics and mechanical properties of calcium silicate hydrate: A molecular dynamics investigation. *Phys. Chem. Chem. Phys.* **2026**, *28*, 9428–9440. [CrossRef] [PubMed]
55. Tang, J.; Zhang, D.; Ma, G.; Ji, X.; Zhou, W. Early Hydration of Calcium Sulfoaluminate Cement at Elevated Temperatures. *ACS Sustain. Chem. Eng.* **2024**, *12*, 13654–13668. [CrossRef]
56. Zhang, R.; Zhao, H.; Lv, G.; Ma, X.; Jiang, X. Advanced ex-situ carbon stabilization technology using municipal solid waste incineration fly ash: A review. *Renew. Sustain. Energy Rev.* **2025**, *218*, 115763. [CrossRef]
57. Lv, Y.; Zhang, K.; Qu, J.; Yin, K.; Yang, C.; Zheng, H.; Xiang, T. Study on physicochemical and anti-corrosion performance of methylsiloxane-based hydrophobic powder modified mortar. *Constr. Build. Mater.* **2024**, *425*, 135999. [CrossRef]
58. Zhu, C.; Li, G.; Wang, J.; Dong, S.; Cao, K.; Lv, Y. Performance improvement in neutron-shielding ultra-high performance mortar prepared with alkaline-treated boron carbide. *J. Build. Eng.* **2023**, *71*, 106435. [CrossRef]
59. Zhu, Y.-G.; Kou, S.-C.; Poon, C.-S.; Dai, J.-G.; Li, Q.-Y. Influence of silane-based water repellent on the durability properties of recycled aggregate concrete. *Cem. Concr. Compos.* **2013**, *35*, 32–38. [CrossRef]
60. Ruan, S.; Chen, S.; Lu, J.; Zeng, Q.; Liu, Y.; Yan, D. Waterproof geopolymer composites modified by hydrophobic particles and polydimethylsiloxane. *Compos. Part B Eng.* **2022**, *237*, 109865. [CrossRef]
61. Lv, Y.; Luo, Y.; Song, C.; Jin, W.; Xiang, T.; Qiao, M.; Dang, J.; Bai, W.; Yang, Z.; Zhao, J. Effect of calcium stearate hydrophobic agent on the performance of mortar and reinforcement corrosion in mortar with cracks. *Constr. Build. Mater.* **2024**, *450*, 138684. [CrossRef]
62. *GB 18598-2019*; Standard for Pollution Control on the Hazardous Waste Landfill. China Environment Publishing Group: Beijing, China, 2019.
63. Marieta, C.; Martín-Garin, A.; Leon, I.; Guerrero, A. Municipal Solid Waste Incineration Fly Ash: From Waste to Cement Manufacturing Resource. *Materials* **2023**, *16*, 2538. [CrossRef] [PubMed]
64. Muhammad, F.; Zhang, B.; Yu, T.; Fahimizadeh, M.; Hassan, M.A.S.; Peng, Z.; Liang, J.; Wei, Y.; Yuan, P. A comprehensive assessment of municipal solid waste incineration fly ash as a cementitious material in limestone calcined clay cement (LC3) for sustainable construction. *Constr. Build. Mater.* **2025**, *494*, 143441. [CrossRef]
65. Ajorloo, M.; Ghodrat, M.; Scott, J.; Strezov, V. Heavy metals removal/stabilization from municipal solid waste incineration fly ash: A review and recent trends. *J. Mater. Cycles Waste Manag.* **2022**, *24*, 1693–1717. [CrossRef]
66. Cui, L.; Chen, X.; Wang, J.; Qiang, Y.; Chen, D.; Xiang, T. Facile preparation of monolithic superhydrophobic concrete with excellent anti-corrosion property. *Mater. Lett.* **2023**, *344*, 134441. [CrossRef]
67. Chen, S.; Lu, P.; Bie, Y.; Wang, L.; Guo, L. Mechanical properties and micro mechanism of alkali-activated tannery sludge/fly ash composite cement-based recycled concrete. *Constr. Build. Mater.* **2023**, *391*, 131813. [CrossRef]
68. Zhao, Y.; Lei, L.; Wang, Q.; Li, X. Study of superhydrophobic concrete with integral superhydrophobicity and anti-corrosion property. *Case Stud. Constr. Mater.* **2023**, *18*, e01899. [CrossRef]
69. Fan, C.; Wang, B.; Zhang, T. Review on Cement Stabilization/Solidification of Municipal Solid Waste Incineration Fly Ash. *Adv. Mater. Sci. Eng.* **2018**, *2018*, 5120649. [CrossRef]
70. Wang, L.; Li, R.-D.; Wei, L.; Li, Y. Accelerated carbonation of municipal solid waste incineration fly ash using CO_2 as an acidic agent for clinker production. *Environ. Eng. Sci.* **2012**, *29*, 677–684.
71. Ruan, S.; Gao, R.; Tu, W.; Li, G.; Lu, J.-X.; Yan, D.; Poon, C.S. Hydration products and hybridisation mechanisms of hydrophobic cement pastes with alkyl-organosilanes. *Cem. Concr. Compos.* **2025**, *163*, 106208. [CrossRef]

72. Yao, S.; Liu, S.; Zou, D.; Pan, C.; Wang, J.; Guan, X.; Zhang, H. Development of an Aerated Sulfoaluminate Cement–Based Material for Coal Mine Filling. *J. Mater. Civ. Eng.* **2023**, *35*, 04022436. [CrossRef]
73. Seo, J.; Kim, S.; Park, S.; Yoon, H.N.; Lee, H.K. Carbonation of calcium sulfoaluminate cement blended with blast furnace slag. *Cem. Concr. Compos.* **2021**, *118*, 103918. [CrossRef]
74. Bizzozero, J.; Gosselin, C.; Scrivener, K.L. Expansion mechanisms in calcium aluminate and sulfoaluminate systems with calcium sulfate. *Cem. Concr. Res.* **2014**, *56*, 190–202. [CrossRef]
75. Lv, Y.; Zhang, K.; Li, J.; Feng, Z.; Jin, W.; Liu, Y. Study on the mechanism of influence of PET, ABS, and steel formworks on the mirror-faced characteristics and physical properties of high-performance mortar surfaces. *Constr. Build. Mater.* **2025**, *499*, 144127. [CrossRef]
76. Meng, Y.; Gao, D.; Yang, L.; Fang, J.; Li, Y.; Zhang, T. Effect of ultra-fine supplementary cementitious materials on the properties of calcium sulfoaluminate cement-based ultra-high performance concrete. *Case Stud. Constr. Mater.* **2024**, *21*, e03547. [CrossRef]